Electrochemical and Solid-State Letters, **9** (8) A390-A394 (2006)
1099-0062/2006/9(8)/A390/5/$20.00 © The Electrochemical Society

SnO_2 Pinning: An Approach to Enhance the Electrochemical Properties of Nanocrystalline $CuFe_2O_4$ for Lithium-Ion Batteries

Ramakrishnan Kalai Selvan,[a] Nallathamby Kalaiselvi,[a,z] Chanassery Ouso Augustin,[a] and Chil-Hoon Doh[b]

[a]*Central Electrochemical Research Institute, Karaikudi 630 006, Tamil Nadu, India*
[b]*Korea Electrotechnology Research Institute, Changwon 641 120, Republic of Korea*

A first attempt to synthesize and explore SnO_2 pinned $CuFe_2O_4$ material as an anode for lithium-ion batteries has been made. The study highlights the approach of exploiting SnO_2 pinning to enhance the electrochemical properties of nanocrystalline $CuFe_2O_4$ anodes. Virgin $CuFe_2O_4$ and SnO_2 pinned $CuFe_2O_4$ powders were synthesized with 10–30 nm via under a one pot solution combustion method with specific calcination conditions. It is further understood that SnO_2 pinning has reduced saturation magnetization and bulk resistance and thereby enhanced the charge-discharge characteristics of native $CuFe_2O_4$ anodes significantly in rechargeable lithium cells.
 [DOI: 10.1149/1.2209435]

Manuscript submitted January 2, 2006; revised manuscript received April 25, 2006. Available electronically June 13, 2006.

Synthesis, characterization, and processing of nanostructured materials are part of the emerging and rapidly growing field of nanotechnology.[1] Of late, a paradigm shift in the area of nanoscience has been observed, especially with respect to the generation of new class of high-performance nanomaterials that connect nanoscience to nanoelectronics and energy devices.[2] Regarding energy devices, it is well known that lithium-ion battery technology is becoming the system of choice to meet the varied requirements of consumer market based energy needs of today. Despite the commercialization of Li-ion batteries, the wider acceptance of carbonaceous anodes is hampered by the large irreversible capacity loss problems. This in turn has opened up new avenues for the deployment of alternate anodes such as mixed metal oxides,[3] metal-metal alloys,[4] SnFe composites,[5] amorphous tin composite oxide anodes,[6] silicon nitrides,[7,8] lithium metal oxides such as $LiMSnO_4$,[9] phosphates,[10] and niobates.[11]

In this direction, spinel-type anodes, viz., Co_3O_4,[12] $CuFe_2O_4$,[13] $CoFe_2O_4$,[14] $NiFe_2O_4$,[15] $ZnFe_2O_4$,[16] and $CaFe_2O_4$[17] have gained prominence due to their high specific capacities and facile synthesis. Their composition, both elemental and stoichiometric, is easily altered without major structural changes, which permits tuning their magnetic and electrochemical properties in a wider range.[18] In addition, bringing the dimensionality of ferrites to a nanometer scale opens up newer windows for applications such as high density memory devices, magnetic resonance imaging contrast agents, drug carriers,[19] and potential electrodes for high capacity and high power Li-ion batteries.[13-17]

Synthesis of size controlled magnetic ferrite anodes for rechargeable lithium batteries is of high scientific and technological interest. Because nanostructured materials obtained through generic routes such as wet chemical, mechanical, form-in place, and gas phase synthesis have significantly different properties depending on the routes chosen to fabricate them,[20] it has been shown that improving the dimensional stability of nanoelectrode materials during Li insertion/extraction cycling is the most vital factor to achieving better cycling performance in lithium-ion batteries.[21] A strategy to enhance the dimensional stability is through uniform pinning of nanosized alloy/oxide into the nanostructured electrode matrix.[21] Based on this, pinning is hereby explored as an effective method to modify bulk electrode properties of $CuFe_2O_4$ anodes for lithium-ion battery applications enabling facile lithium diffusion through porous internal and external surfaces. This approach of SnO_2 pinning upon $CuFe_2O_4$ anodes offers excellent dimensional and structural stability upon extended cycling compared to the conventional geometric and electronic modifications of the surface of native $CuFe_2O_4$ material.

In this work, a modified one-pot solution combustion method has been adopted for the synthesis of $CuFe_2O_4$ and SnO_2 (5 wt %) pinned $CuFe_2O_4$ with the structure of discrete nanoparticles. This method is versatile enough, easily scalable and provides high product yield. Besides being a first attempt to report on the pinning of $CuFe_2O_4$ matrix with SnO_2, the present study paves the way to understanding the effect of pinning and the role of pinned SnO_2 in enhancing the electrochemical properties of nano$CuFe_2O_4$ anodes. Toward this, the electrochemical performance of the (5 wt %) SnO_2 pinned $CuFe_2O_4$ has been compared with the native $CuFe_2O_4$ anodes to have better insights on the aforesaid factors. Thus the present study is a first attempt to explore SnO_2 as a pinning agent over ferrite electrode and the adoption of simple solution assisted combustion method to achieve the process of pinning by a unique approach. It is well known that the literature is replete with the protective copper layer on the surface of tin based electrodes to improve the electrochemical characteristics of the latter.[23] On the other hand, the present study highlights the importance and significance of the reverse formulation, i.e., effect of SnO_2 pinning on $CuFe_2O_4$ electrode toward modifying the electrochemical properties of virgin nano$CuFe_2O_4$ anodes for use in rechargeable lithium batteries.

Experimental

The nanocrystalline $CuFe_2O_4$ and SnO_2 pinned $CuFe_2O_4$ were prepared by urea-nitrate combustion method. Stoichiometric quantities of $Cu(NO_3)_2 \cdot 6H_2O$ and $Fe(NO_3)_3 \cdot 9H_2O$ dissolved in water were treated with a solution containing a mixture of $SnCl_4$ in HNO_3 and $CO(NH_2)_2$ in distilled water. The resultant homogeneous solution was oven dried at 110°C to obtain amorphous precursors prior to furnace calcination to ensure nanoparticle size optimization and uniform filling of micropores of $CuFe_2O_4$ matrix by SnO_2. In addition, a slow rate of furnace heating (5°C/min) was applied to the precursors up to 300°C (24 h) initially and 750°C (3 h) thereafter, with intermittent grinding. Finally, the ultrafine powders were heated to 1100°C at a heating rate of 10°C/min for ~5 h to obtain highly crystalline copper ferrite pinned with SnO_2. Heating sequences from 110 to 1100°C with an appropriate rate of heating was expected to offer systematic pinning of SnO_2 (in the form of cavity trapped moiety) without forming any structural defects or defaults in $CuFe_2O_4$ matrix, i.e., the slow rate of evaporation of excess of water at 110°C is accompanied by the formation of solid precursors wherein SnO_2 particles are dripped into the invisible pores of virgin $CuFe_2O_4$. Upon heating to 300°C, the trapped SnO_2 particles align themselves to have tight packing, the so-called pin-

[z] E-mail: kalakanth2@yahoo.com

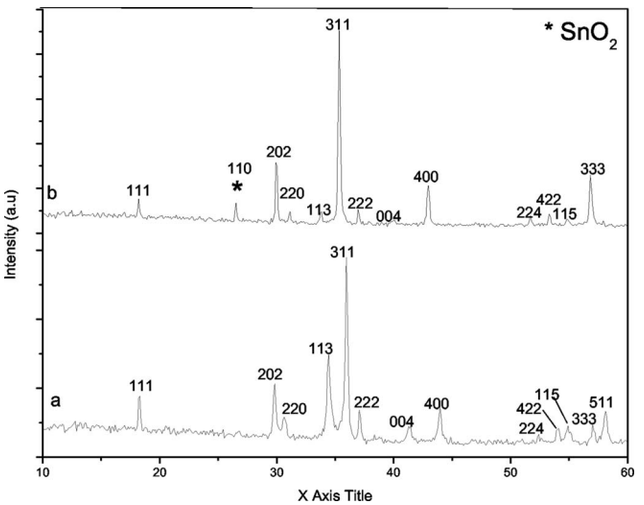

Figure 1. XRD patterns of (a) $CuFe_2O_4$ and (b) SnO_2 pinned $CuFe_2O_4$.

ning inside the mesopores of $CuFe_2O_4$, thus attain visibility in X-ray diffraction (XRD) and high-resolution transmission electron microscope (HRTEM) also. The procedure for the electrode fabrication, instrumental details of charge discharge, TEM, and HRTEM are given elsewhere.[11,22] Magnetic measurements were taken on a magnetic property measurement system superconducting quantum interference device (SQUID). The ac impedance measurements were made at room temperature using a HIOKI 353 impedance analyzer controlled by a computer in the frequency range of 42 Hz to 5 MHz at zero potential. The samples were prepared by making pellets with 1 cm diam and 0.2 cm thickness using a hydraulic press applying 3.5 tons/cm^2 pressure. Silver paint was coated on both sides of the pellet to act as a blocking electrode.

Results and Discussion

The XRD patterns of nanocrystalline $CuFe_2O_4$ and nanoSnO_2 pinned $CuFe_2O_4$ powders are shown in Fig. 1. Figure 1a demonstrates the presence of sharp and well-defined peaks corresponding to the spinel structure of $CuFe_2O_4$ without any impure phase. From the peak pattern recorded, it is deduced that the synthesized $CuFe_2O_4$ possesses a tetragonal structure with the lattice parameters of $a = 8.2740 \pm 0.02$ Å and $c = 8.4814 \pm 0.03$ Å (PDF no. 6-545). On the other hand, the XRD pattern of SnO_2 pinned $CuFe_2O_4$ (Fig. 1b) shows an extra peak (110) confirming the presence of SnO_2. Subsequently, a change in the calculated lattice parameter values of $CuFe_2O_4/SnO_2$ has been observed, denoting a possible phase transition from tetragonal to cubic ($a = 8.4125 \pm 0.02$ Å). Such a change is attributed to the effect of added SnO_2 due to the difference in ionic radii ($Sn^{4+} = 0.69$ Å and $Fe^{3+} = 0.65$ Å). It is amazing that unlike the surface coated electrodes, a peak due to SnO_2 is seen in the XRD of SnO_2 pinned $CuFe_2O_4$ (Fig. 1b), which is an indication that SnO_2 is not only coated on the surface, but also has entered into the bulk structure of nano$CuFe_2O_4$, known as pinning of SnO_2.[24]

Note that the detrimental presence of γ-Fe_2O_3 as an unavoidable impurity to produce copper stannate has been successfully overcome in the present study, by the adoption of solution assisted combustion method with specific heating sequences. This substantiates the single-phase formation of SnO_2 pinned $CuFe_2O_4$, since no peak corresponding to copper stannate is obtained in the XRD pattern (Fig. 1b). Another important observation is that $CuFe_2O_4/SnO_2$ material with cubic symmetry and native $CuFe_2O_4$ with tetragonal symmetry have been synthesized in their crystalline and discrete nanometric forms by adopting solution assisted combustion method, which is the highlight of the present work.

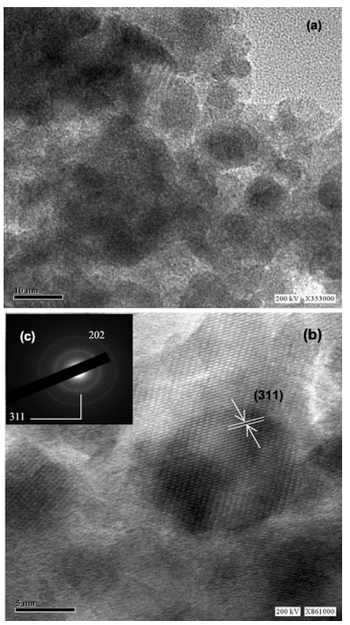

Figure 2. (a) TEM, (b) HRTEM, and (c) SAED images of nanocrystalline $CuFe_2O_4$.

Fig. 2a shows the TEM images of copper ferrite nanoparticles, wherein the particles are found to be poly dispersed with a particle size in the range between 10 and 20 nm. This result is fairly consistent with the values evaluated from XRD. It is obvious that the ferrite nanoparticles possess uniform size and shapes, even though no size selection has been made in the as-synthesized particles. The presence of nanoscale ferrite particles with embedded nanoSnO_2 is evident from Fig. 3a. Generally, cubic shape is reported to be formed, in the presence of weakly binding capping molecules,[25] whereas, strongly binding pinning molecules would lower the par-

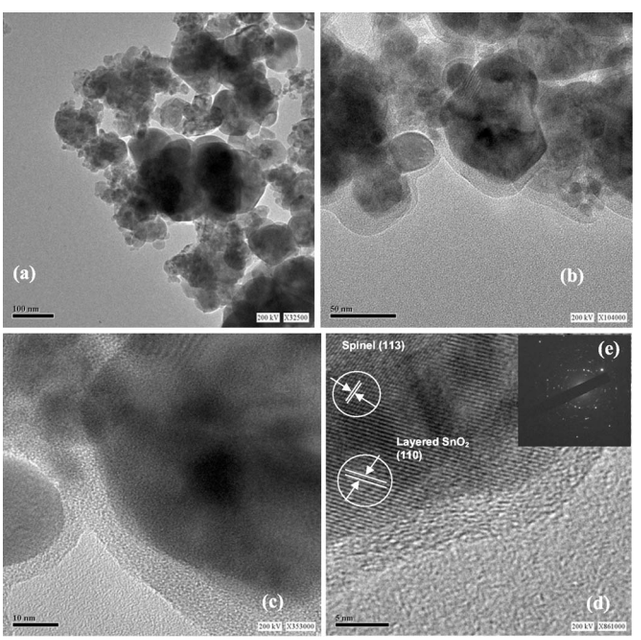

Figure 3. (a–c) TEM, (d) HRTEM, and (e) SAED images of SnO_2 pinned $CuFe_2O_4$.

ticle size and will lead to spherical shaped nanoparticles. The same is observed in the present study due to the strong pinning of SnO_2 (Fig. 3a-d).

The HRTEM images of $CuFe_2O_4$ (Fig. 2b) confirmed the well-defined lattice fringes with a definite "d" value of 2.51 Å, which corresponds to the prominent (311) plane for copper ferrite. Similarly, the presence of SnO_2 phase in the ferrite bulk material is confirmed from Fig. 3d, as it corresponds to $CuFe_2O_4$ spinel (113) with a "d" value of 2.63 Å and layered SnO_2 (110) with a "d" value of 3.38 Å which are structurally integrated to offer structural compatibility and stability to the pinned ferrite matrix. Hence, it is confirmed from HRTEM (Fig. 3d) also that the SnO_2 particles are tightly pinned on the surface as well as penetrated into the nanopores of $CuFe_2O_4$ electrode material as evidenced already from XRD.

Selected area electron diffraction (SAED) pattern of $CuFe_2O_4$ measured from a large zone presents rings (Fig. 2c) that can be indexed to a single crystal structure. On the other hand, bright spots are seen in HRTEM of SnO_2 pinned $CuFe_2O_4$ (Fig. 3e) due to the presence of SnO_2 nanoparticle embedded in the (Li ion conducting) $CuFe_2O_4$ nanophase to exhibit polycrystalline structure. It is reported that the additional intrawall space (obvious from Fig. 3c and d) not only can provide extra routes for Li^+ transport/insertion, but can also enhance the dimensional stability of pinned ferrite matrix.[26] Moreover, flexible thin wall structures of the pinned SnO_2 (Fig. 3d) would allow a more efficient Li^+ ion diffusion from both exterior and interior surfaces, resulting in a more symmetric volume transport and a large charge storage. As a result, enhanced electrochemical activity is expected for SnO_2 pinned $CuFe_2O_4$ anodes compared to the native $CuFe_2O_4$ anode, which is realized in the charge-discharge characteristics of ferrite anodes.

Prior to electrochemical evaluation, the magnetic properties of ferrite anodes were investigated with a view to understand the impact of SnO_2 pinning upon magnetic properties. The magnetization of $CuFe_2O_4$ and SnO_2 pinned $CuFe_2O_4$ with varying applied field has been studied using SQUID magnetometer at ambient temperature. The SnO_2 pinned $CuFe_2O_4$ exhibited reduced saturation magnetization (Ms) of 11 emu/g against 30 emu/g observed for virgin $CuFe_2O_4$. The reduction of Ms value is attributed to the effect of pinning wherein SnO_2 is impregnated at the interface of ferrite matrix along with pinning of surface of spins,[27] that is in accordance with the XRD and HRTEM observations discussed earlier.

The electrochemical behavior of native $CuFe_2O_4$ and SnO_2 pinned $CuFe_2O_4$ anodes were studied against lithium metal in 2016 coin cells by performing several charge discharge cycles under galvanostatic conditions using 0.05 mA current (Fig. 4 and 5). The voltage plateau observed around 0.7–0.8 V corresponds to the reduction reactions of Fe^{3+} and Cu^{2+} with lithium during the first discharge of $CuFe_2O_4$ electrode.[28] Another voltage plateau observed at 0.2 V during the first discharge of SnO_2 pinned $CuFe_2O_4$ is due to the intercalation of Li with the pinned SnO_2 upon discharge,[29,30] thus confirms the presence of SnO_2 moiety into the $CuFe_2O_4$ matrix. One more interesting observation is that the voltage at which charge-discharge occurs during the second and successive cycles is higher (>0.9 V) than the first cycle discharge process of both native and SnO_2 pinned copper ferrites. This enhanced voltage behavior could be assigned to the poorly crystalline nature of the reduced product obtained from the redox reactions of the first cycle.[15] i.e., similar to the reported charge discharge behavior of $CoFe_2O_4$ anodes,[14] amorphization process of $CuFe_2O_4$ takes place during the first discharge (0.7–0.8 V) that results in the transformation of nanocrystalline spinel ferrite structure to amorphous phase. This process is accompanied by an irreversible reduction of amorphous $CuFe_2O_4$ with lithium to form metallic Cu, Fe, and Li_2O as products according to[14]

$$8Li + CuFe_2O_4 \rightarrow Cu + 2Fe + 4Li_2O \qquad [1]$$

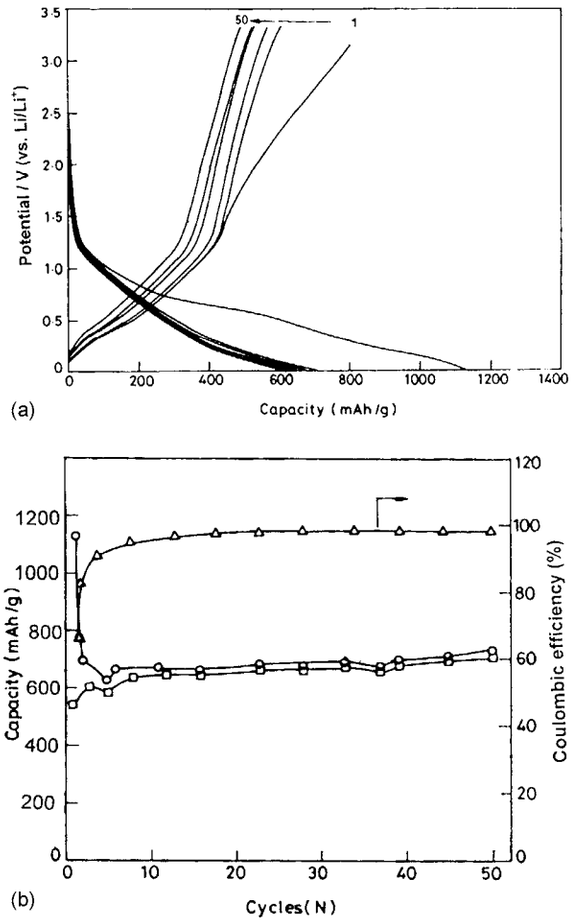

Figure 4. (a) Charge-discharge behavior of Li/$CuFe_2O_4$ cells and (b) capacity *vs* cycleability behavior of $CuFe_2O_4$ anode in Li/$CuFe_2O_4$ cell.

However a reversible oxidation/reduction takes place subsequently according to

$$4Li_2O + Cu + 2Fe \leftrightarrow CuO + Fe_2O_3 + 8Li \qquad [2]$$

As a result, the oxidation and reduction processes of transition metals in copper ferrite account for the observed high specific capacity values ($\sim$1200 mAh/g) of $CuFe_2O_4$ anodes upon cycling. In other words, the reversible reactions of $Cu^{2+} \rightarrow Cu^o$ and $Fe^{3+} \rightarrow Fe^o$ contribute to the extraordinary higher specific capacity values ($>$1000 mAh/g) of nano $CuFe_2O_4$ anodes (Fig. 4a).

Also, the observed high capacity values may be attributed to the maximum lithium uptake [of 8 Li per formula (915 mAh/g) and the irreversible reactions of the electrode materials with the electrolytes. This in turn would form a passive layer over the surface of ferrite electrodes as reported in the literature.[15] Subsequently, an experimentally reversible capacity of 780 mAh/g has been measured from the charging reaction of the first cycle, thus accounts for significant irreversible capacity loss ($\sim$33%) behavior of the $CuFe_2O_4$ anode. The first cycle irreversibility capacity loss of $CuFe_2O_4$ may be due to the loss of contact between binder and electrode material that results from volume and structural variation of active material upon cycling. This critical issue has also been solved by SnO_2 pinning by way of enhancing contact between ferrite particles, binder, and with the trapped SnO_2 moiety. The advantages of SnO_2 pinning over $CuFe_2O_4$ matrix is obvious from the reduced first cycle irreversible capacity values (11%) of SnO_2 pinned ferrite anode, i.e., the first cycle Q_{dc} ($\sim$1153 mAh/g) and Q_c ($\sim$950 mAh/g) values of SnO_2 pinned $CuFe_2O_4$ anode (Fig. 5) do not differ much from each other,

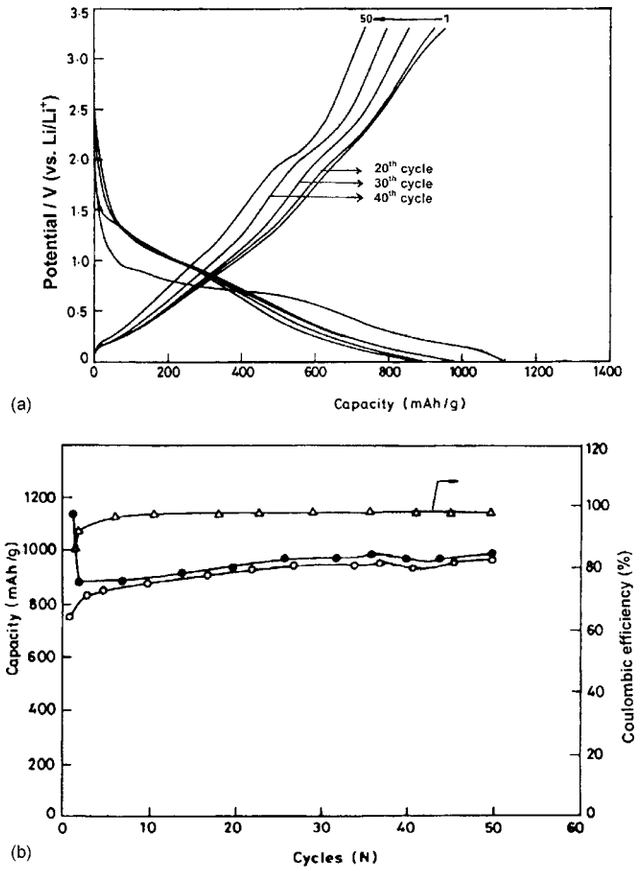

Figure 5. (a) Charge-discharge behavior of Li/SnO_2 pinned $CuFe_2O_4$ cells and (b) capacity vs cycleability behavior of SnO_2 pinned $CuFe_2O_4$ anode in Li-ion cells.

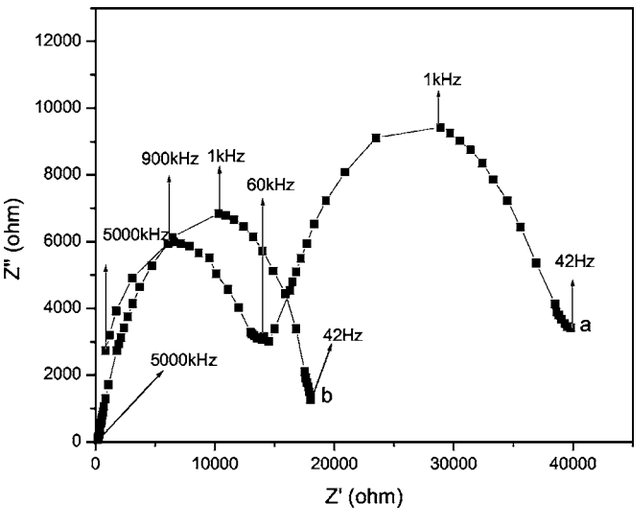

Figure 6. Impedance spectra of (a) $CuFe_2O_4$ and (b) SnO_2 pinned $CuFe_2O_4$ recorded at zero potential.

an indication of better Coulombic efficiency (85%) and better cycling performance. However, based on the permissible first cycle irreversible capacity values observed for both the anodes (Fig. 4a and 5a), the possibility of considering alloy-forming mechanism is ruled out. As a result, charge-discharge behaviors of ferrite-based anodes of the present study are believed to follow displacive redox mechanism according to Eq. 1 and 2, which is similar to those of metal oxide anodes.[13-17]

The observed high specific capacity values and the possible involvement of displacive redox mechanism for the charge-discharge behavior of ferrite anodes are further understood from the following discussion also. Generally, anodes containing Li_2O are reported to deliver capacities slightly higher than those without Li_2O, suggesting that the formed/added Li_2O accelerated lithium extraction from the amorphous anode materials.[31] Similarly, it is believed that the diffusion of lithium into the amorphous material with Li_2O must be faster, provided the morphology of the particle in both cases is of nanoscale. This holds good for the chosen category of nanoferrite and SnO_2 pinned ferrite anodes of the present study to exhibit significantly higher specific capacity values. Similarly, the formation of Li_2O is possible only through redox mechanism and so it is confirmed that the ferrite anodes follow displacive redox mechanism as described already.

Basically, prevention of nanoscale alloy/metal particles from contacting with the electrolyte solution is necessary for avoiding the formation of unstable SEI film which is one of the reasons for the low Coulombic efficiency ($\sim$65%) observed in the first cycle of the native $CuFe_2O_4$ anode (Fig. 4b). A possible solution to this problem is that all micromesopores of the electrode material should be plugged by the coating materials to prevent unstable SEI film formation, agglomeration, and pulverization of particles of the electrode active materials.[32] In SnO_2 pinned $CuFe_2O_4$ electrodes, SnO_2 that is strongly bonded to the copper ferrite particle matrix acts as fillers of micromesopores and inhibits particle aggregation[32] even upon extended cycling.[33] Consequently, SnO_2 pinned ferrite nanoparticles significantly reduce the formation of surface cracks induced from the volume changes and thereby diminish the repetitive formation of electrode/electrolyte interfaces that affect the capacity fading.

Also, enhanced electrochemical performance due to SnO_2 pinning is attributed to the limited oxygen content in the mixture, which consumes optimum amounts of lithium for the irreversible formation of Li_2O to offer lower irreversible capacity (Fig. 5a). As a result, SnO_2 pinned $CuFe_2O_4$ anode possesses significant cyclic reversibility than native $CuFe_2O_4$ anodes with an acceptable fading capacity values (11%) upon ambient temperatures cycling (up to 50 cycles) (Fig. 5b). In other words, SnO_2 pinning is found to enhance the first cycle Colombic efficiency of ferrite anodes from 65 to 85%, which is the major advantage of SnO_2 pinning.

Further the improved electrochemical behavior of SnO_2 pinned ferrite is substantiated by the decreased bulk resistance observed for SnO_2 pinned $CuFe_2O_4$ material compared to the virgin $CuFe_2O_4$ powders as evident from Fig. 6. From the figure, it is evident that the impedance spectrum of native $CuFe_2O_4$ shows two semicircles corresponding to grain and grain boundary effect. It is understood that in the high-frequency region the conduction mechanism is predominant for grain boundary effect and in the low-frequency region, the same is due to grain effect. On the other hand SnO_2 pinned $CuFe_2O_4$ shows only one semicircle, an indication that the conduction mechanism due to grain effect is predominant. Also the absence of grain boundary effect in the SnO_2 pinned ferrite sample is attributed to the enhanced particle size[34] of 20–30 nm (Fig. 3b) compared with the parent $CuFe_2O_4$ (10 nm) as evident from the Fig. 2a. Furthermore, it is well known that the decreased bulk resistivity of SnO_2 pinned copper ferrite would enhance the inherent ionic conductivity of the same.[35] As a result, an enhanced Li^+ ion diffusion kinetics is expected, when the SnO_2 pinned copper ferrite electrode (prepared with the examined powders) is deployed as an anode in lithium-ion cells and subjected to charge-discharge characteristics. This in turn would improve the electrochemical properties of the synthesized nanocrystalline $CuFe_2O_4$ anodes both in terms of higher specific capacity ($>$1000 mAh/g) and better cyclability with acceptable capacity fade ($>$20%).

Despite the remarkably enhanced electrochemical characteristics of SnO_2 pinned $CuFe_2O_4$ anodes compared to the native $CuFe_2O_4$ anode, one cannot ignore the observed irreversible capacity values of ~300 mAh/g that has been encountered during the second cycle. i.e., such a huge difference in the observed specific capacity values between the first and second cycles that arises due to the reduction of SnO_2 to metallic Sn and $2Li_2O$ and the formation of surface films need to be minimized significantly. Toward this, certain reported remedial measures of the following type could be adopted with a view to minimize the initial capacity loss problems. Reduction of SnO_2 in the pores prior to electrochemical cell assembly,[36] formation of passivating surface films that can cover the microcavities in their outer side to protect the pinned particles inside,[36] better management of pores, which are being filled up with tin oxide via confinement of smaller and appropriate pores to avoid detrimental reactions with electrolyte,[36] deployment of electrodes containing electroactive materials with optimized particle size to facilitate lithium insertion/extraction, and[37] optimization of various parameters such as heat treatment of active materials, composition of electrolyte solution, amount of carbon and/or binder added towards the fabrication of electrode.[38]

In addition, similar to the reported suggestions to improve the irreversible capacity loss problems of nonlithiated metal oxide anodes,[3] prelithiation of native $CuFe_2O_4$, and SnO_2 pinned $CuFe_2O_4$ via chemical or electrochemical methods to address the requirement of excess of total internal lithium supply as a means of reducing the initial capacity loss may also be attempted, since the major source of lithium is the cathode in both the metal oxide and ferrite anode based Li-ion batteries. Furthermore, exploring the possibility of pinning SnO_2/lithiated SnO_2[39] into native $CuFe_2O_4$ matrix through suitable electrochemical techniques would also bring more light toward the understanding of probable reasons and remedial measures pertaining to the minimization of initial irreversible capacities of SnO_2 pinned $CuFe_2O_4$ anodes.

Conclusions

Using simple solution combustion method, single phase and nanometric $CuFe_2O_4$ and SnO_2 pinned $CuFe_2O_4$ anode materials have been synthesized. Pinning of SnO_2 on the surface and inside the nanopores of $CuFe_2O_4$ materials has been evidenced by HRTEM, which in turn has significantly modified the bulk electrode properties of $CuFe_2O_4$ anodes in rechargeable lithium batteries, i.e., the higher charge-discharge capacity, lower irreversible capacity, and better cycling stability of the modified $SnO_2/CuFe_2O_4$ electrode are attributed to SnO_2 pinning. The enhanced cycling performance can also be attributed to Li^+ ions having multiple entrances/exits during charge and discharge, which includes porous internal and external surfaces as well as sphere openings created via SnO_2 pinning. Also, the strongly pinned SnO_2 particles impart structural stability to the $CuFe_2O_4$ matrix and maintained upon extended cycling, which is considered as yet another factor responsible for the extended cycle life behavior of SnO_2 pinned $CuFe_2O_4$ with excellent Colombic efficiency.

Acknowledgments

The authors thank Professor A. Gedanken, Bar-Ilan University, Israel for providing TEM and HRTEM analysis. The authors are also grateful to Professor A. K. Shukla, Director, CECRI for his keen interest.

The Central Electrochemical Research Institute assisted in meeting the publication costs of this article.

References

1. Z. Tang and N. A. Kotov, *Adv. Mater. (Weinheim, Ger.)*, **17**, 951 (2005).
2. C. N. R. Rao and A. K. Cheetham, *J. Mater. Chem.*, **11**, 2887 (2001).
3. P. Polzot, S. Laruella, S. Grugeon, L. Dupont, and J. M. Tarascon, *Nature (London)*, **407**, 496 (2000).
4. J. Xie, X. B. Zhao, G. S. Cao, Y. D. Zhong, M. J. Zhao, and J. P. Tu, *Electrochim. Acta*, **50**, 1903 (2005).
5. O. Mao, R. L. Turner, I. A. Courtney, B. D. Fredericksen, M. I. Buckett, L. J. Krause, and J. R. Dahn, *Electrochem. Solid-State Lett.*, **2**, 3 (1999).
6. T. Prem Kumar, R. Ramesh, Y. Y. Lin, and G. T. K. Fey, *Electrochem. Commun.*, **6**, 520 (2004).
7. M. Green, E. Fielder, B. Scrosati, M. Wachtler, and J. S. Moreno, *Electrochem. Solid-State Lett.*, **6**, A75 (2003).
8. M. Nishijma, Y. Takeda, N. Imanishi, and O. Yamamota, *J. Solid State Chem.*, **113**, 205 (1994).
9. C. H. Doh, N. Kalaiselvi, C. W. Park, B. S. Jin, S. I. Moon, and M. S. Yun, *Electrochem. Commun.* **6**, 965 (2004).
10. M. V. V. M. Satya Kishore, U. V. Varadaraju, and B. Raveau, *J. Solid State Chem.*, **77**, 3981 (2004).
11. N. Kalaiselvi, C. H. Doh, C. W. Park, S. I. Moon, and M. S. Yun, *Electrochem. Commun.*, **6**, 1110 (2004).
12. J. T. Son, *Electrochem. Commun.* **6**, 990 (2004).
13. W. Y. Li, L. N. Xu, and J. Chen, *Adv. Funct. Mater.*, **15**, 851 (2005).
14. Y. Q. Chu, Z. W. Fu, and Q. Z. Qin, *Electrochim. Acta*, **49**, 4915 (2004).
15. R. Alcántara, M. Jaraba, P. Lavela, J. L. Tirado, J. C. Jumas, and J. O. Fourcade, *Electrochem. Commun.*, **5**, 16 (2003).
16. Y. N. NuLi, Y. Q. Chu, and Q. Z. Qin, *J. Electrochem. Soc.*, **151**, A1077 (2004).
17. N. Sharma, K. M. Shaju, G. V. Subba Rao, and B. V. R. Chowdari, *J. Power Sources*, **124**, 204 (2003).
18. Z. R. Dai, Z. W. Pan, and Z. L. Wang, *Adv. Funct. Mater.*, **13**, 9 (2003).
19. P. Tartaj, M. P. Morales, S. V. Verdaguer, T. G. Carreno, and C. J. Serna, *J. Phys. D*, **36**, R182 (2003).
20. M. J. Pitykethly, *Mater. Today*, **7**, 20 (2004).
21. H. Li, Q. Wang, L. Shi, L. Chen, and X. Huang, *Chem. Mater.*, **14**, 203 (2002).
22. R. Kalai Selvan, C. O. Augustin, C. Sanjeeviraja, V. G. Pol, and A. Gedanken, *Mater. Chem. Phys.*, In press.
23. W. Pu, X. He, J. Ren, C. Wan, and C. Jiang, *Electrochim. Acta*, **50**, 4140 (2005).
24. H. W. Ha, K. H. Jeong, N. J. Yun, M. Z. Hong, and K. Kim, *Electrochim. Acta*, **50**, 3764 (2005).
25. M. Noh, Y. Kim, M. G. Kim, H. Lee, H. Kim, Y. Kwon, Y. Lee, and J. Cho, *Chem. Mater.*, **17**, 3320 (2005).
26. Y. Wang, J. Y. Lee, and H. C. Zeng, *Chem. Mater.*, **17**, 3899 (2005).
27. S. Si, C. Li, X. Wang, D. Yu, Q. Peng, and Y. Li, *Cryst. Growth Des.*, **5**, 391 (2005).
28. Y.-N. NuLi and Q.-Z. Qin, *J. Power Sources*, **142**, 292 (2005).
29. A. Caballero, J. Morales, and L. Sanchez, *Electrochem. Solid-State Lett.*, **8**, A464 (2005).
30. N. Sharma, J. Plevert, G. V. Subba Rao, B. V. R. Chowdari, and T. J. White, *Chem. Mater.*, **17**, 4700 (2005).
31. A. Sivashanmugam, T. Prem Kumar, N. G. Renganathan, S. Gopukumar, M. W. Mehrens, and J. Garche, *J. Power Sources*, **144**, 197 (2005).
32. H. Li, Q. Wang, L. Shi, L. Chen, and X. Huang, *Chem. Mater.*, **14**, 103 (2002).
33. C. Kim, M. Noh, M. Choi, J. Cho, and B. Park, *Chem. Mater.*, **17**, 3297 (2005).
34. V. Thangadurai and W. Weppner, *J. Solid State Chem.*, **179**, 974 (2006).
35. M. S. Bhuvaneswari, S. Selvasekarapandian, S. Fujihara, and S. Koji, *Solid State Ionics*, **177**, 121 (2006).
36. I. Grigoriants, A. Soffer, G. Salitra, and D. Aurbach, *J. Power Sources*, **146**, 185 (2006).
37. H. J. Ahn, H. C. Choi, K. W. Park, S. B. Kim, and Y. E. Sung, *J. Phys. Chem.*, **108**, 9815 (2004).
38. J. Zhu, Z. Lu, S. T. Aruna, D. Aurbach, and A. Gedanken, *Chem. Mater.*, **12**, 2557 (2000).
39. D. Aurbach, A. Nimberger, B. Markovsky, E. Levi, E. Sominski, and A. Gedanken, *Chem. Mater.*, **14**, 4155 (2002).